#### TECHNICAL ARTICLE

# Two-Step Isothermal Bainitic Transformation in Medium-Carbon Low-Si Steels with Exceptional Mechanical Properties and Wear Resistance

W.Y. Ren, Z. Zhang, J. Zhang, R. Yang, C.S. Yu, P.K. Liaw, Y.C. Wu, and J.W. Qiao

Submitted: 21 November 2022 / Revised: 11 December 2022 / Accepted: 21 December 2022

The effects of the conventional isothermal bainitic transformation (CIT), two-step isothermal bainitic transformation (TIT) on the microstructure, mechanical behavior, and wear resistance of a medium-carbon low-Si steel were investigated. For the bainite reaction, it is well known that the bainite-plate size decreases as the transformation temperature is reduced. In comparison with the CIT, TIT produced finer bainitic ferrite plates with finer carbides, and an optimum combination of strength, ductility, and impact toughness (an ultimate tensile strength of 1500 MPa, total elongation of 8.6%, and V-notch impact value of 42 J), the wear rate is calculated to evaluate its wear performance, and the wear rates of a CIT sample and TIT sample were  $0.36 \times 10^{-4}$  and  $1.46 \times 10^{-4}$  mm<sup>3</sup> N<sup>-1</sup> m<sup>-1</sup>, respectively.

Keywords

low-Si steels, mechanical properties, microstructure, two-step super-bainite, wear resistance

#### 1. Introduction

Nanobainite steels have received much attentions since they were first discovered by Bhadeshia et al. (Ref 1-4). The key to the strength/hardness—toughness combination depends on the ultrafine bainite and retained austenite (Ref 1). The presence of a nanoscale bainitic microstructure and very high dislocation density are the reason why the nanobainite steels have ultrahigh strength, whereas film-like austenites that exist between bainite-ferrite plates provide good ductility at room temperature (Ref 1, 4). In addition, the excellent wear properties have been found which were attributed to the austenitization and the martensite transformation of the surface layer during abrasion (Ref 5-8).

Bainite steels are composed of residual austenites (*RAs*) and bainites (Ref 9), and there are two forms of retained austenite in bainitic steels. One is film-like retained austenites (*FRAs*), and the other is block-like retained austenites (*BRAs*), which tend to transform into brittle martensites (Ref 10, 11), reducing the toughness of bainite steels (Ref 12-15). Bhadeshia et al. (Ref 12, 13) pointed out that the steels would exhibit a relatively good toughness–strength combination when the ratio of file-like retained austenites to block-like retained austenites was

W.Y. Ren, Z. Zhang, Y.C. Wu, and J.W. Qiao, College of Materials Science and Engineering, Taiyuan University of Technology, Taiyuan 030024, China; J. Zhang, R. Yang, and C.S. Yu, Zhejiang Laifual Drive Co., Ltd., Shaoxing 312462 Zhejiang, China; P.K. Liaw, Department of Materials Science and Engineering, The University of Tennessee, Knoxville, TN 37996-2200. Contact e-mails: zhangzheng1980@126.com and qiaojunwei@gmail.com.

larger than 0.9. And it follows that the criterion for performance optimization is that

$$(V_{\text{FRA}}/V_{\text{BRA}}) = V_{\text{b}}/(6 - 7.7V_{\text{b}}) > 0.9$$
 (Eq 1)

where  $V_{\text{FRA}}$  is the volume fraction of film-like retained austenites,  $V_{\text{BRA}}$  is the volume fraction of the blocky retained austenites, and  $V_b$  is the volume fraction of bainitic ferrites. From Eq 1, it seems that the larger the ratio of the retained austenite and blocky retained austenite, the better the mechanical properties of bainite steels. According to  $T_0$  [the temperature, which the austenites and ferrites with the same chemical composition have the same free energy (Ref 1, 9, 16)] curve, a greater volume fraction can be obtained by decreasing the bainite transformation temperature. It is due to that the block austenites transform into bainites and decompose into film-like austenites at lower temperatures. Bainites generated at a lower temperature are usually finer (Ref 17, 18), which is beneficial to improve the strength (Ref 19). Moreover, prior studies (Ref 20, 21) implicate that the lower austempering temperature, the better wear resistance of the bainitic steels. So, it is necessary to perform austempering at low temperatures to obtain ultrafine bainites and more film-like retained austenites. Ultrafine bainites can be obtained by one-step bainite transformation in high-C high-Si steels (Ref 1, 2). For (low) medium-carbon high-Si steels, a multi-step isothermal treatment has been introduced to produce ultrafine bainites (Ref 22-27). Generally, when the bainitic transformation occurs, it would result in further carbon enrichment in remaining austenites (Ref 9) and lower the  $M_{\rm S}$  temperature sufficiently to be able to conduct the next step of the isothermal bainitic heat treatment at lower temperatures. However, only a few researchers performed the multi-step isothermal bainite transformation on low-silicon steels, and the goal of this study is to investigate the influence of two-step isothermal bainitic transformation (TIT) on the mechanical properties and wear resistance of medium-carbon low-Si steels.

# 2. Experimental

A commercial AISI 4340 steel sheet with the dimensions of  $80 \times 16 \times 15$  mm was selected for this investigation. The chemical composition of this steel was Fe-0.4C-0.61Mn-0.35Si-0.85Cr-1.46Ni-0.26Mo in weight percent (wt.%). The heat treatment cycle used in the present work is shown in Fig. 1. The samples 1 was firstly austenitized at 960 °C for 1 h, followed by rapid quenching in a salt bath that was held at 320 °C and then kept at this salt-bath temperature for 4 h to obtain a conventional bainitic structure (i.e., the conventional isothermal sample) and finally quenched in water. In contrast to the simple 1, the sample 2 was isothermally transformed at 320 °C for 10 min (the same austenitizing temperature and time as the sample 1) to obtain partial bainites and then was immediately moved to another furnace where it was kept at 270 °C for 10 h (a two-step process, designed for the superbainite transformation).

The metallographic samples were mounted and polished with various sandpapers (grit numbers from 600 up to 2000) after the heat treatment. To differentiate lower bainites and martensites and estimate the phase volume fraction, a solution of 10 vol.% sodium metabisulfite solution was used to etch the samples, and then the samples were observed by optical microscopy (OM, DM6000M). The image Pro plus 6.0 (Ref 28) was used to measure the volume fraction of bainites while the microstructure observation of the as-prepared samples etched with a 4 vol.% Nital solution was performed by scanning electron microscopy (SEM, PHENOMWRLD, 15 kV). Moreover, the thin foil samples for transmission electron microscope (TEM) observations were prepared by a twinjet polishing technique, using an electrolyte containing 10% perchloric acid and 90% methanol electrolyte in volume percent, and the details of microstructures were observed by a JEM-2100F TEM. X-ray diffraction (XRD), employing filtered Co Ka radiation with an acceleration voltage of 40 kV and current of 40 mA, was utilized to determine the amount of retained austenites (RAs).

Vickers hardness was measured, using the heat-treated samples with a Vickers hardness tester at 200 gf for 9 s. The Vickers hardness was determined for ten times for each sample, and the average value was obtained.

Instron 5969 equipped with an extensometer at a strain rate of  $10^{-3}$  s<sup>-1</sup> was employed to assess the room-temperature tensile properties.

The impact toughness was conducted on a JBW-500 machine, using standard Charpy V-notched specimens, and all the values were the average of three tests.

Furthermore, the wear resistance experiments were performed on a universal wear-testing machine (HT-4001, China) at the applied normal loads of 10 N. The volume loss owing to wear is defined by:

$$\Delta V = Lh(3h^2 + 4b^2)/(6b)$$
 (Eq 2)

where  $\Delta V$  is the volume loss, L is the length of the wear track, and b and h are the width and depth of the wear scars, respectively. The following equation was used to calculate the wear rate:

$$W_{\rm r} = \Delta V/(PS) \tag{Eq 3}$$

where  $W_{r}$ , P, and S are the wear rate, the normal load applied, and the total sliding distance, respectively.

# 3. Results

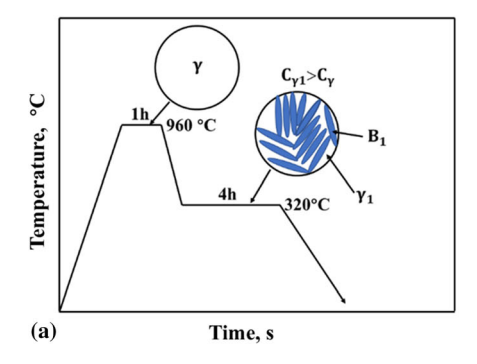
## 3.1 The Determination of $M_S$ , $M_{S2}$

The martensitic-start temperature ( $M_{\rm S}$ ) is calculated by the MUCG83 software (Ref 23) developed by Bhadeshia at Cambridge University, and the calculated  $M_{\rm S}$  temperature is 310 °C. Besides, the time–temperature transformation (TTT) diagram was determined by the MUCG83 thermodynamic model, as shown in Fig. 2. The TTT diagram consists of two upper and lower C curves predicting the kinetics of the reconstructive and shear transformations, respectively (Ref 27). Moreover, in order to determine the two-step bainite isothermal treatment temperature,  $M_{\rm S2}$  (the martensitic start temperature of the untransformed austenites) is calculated, using the following empirical equations (Ref 29).

$$X_Y = (\bar{x} - V_b x_b)/(1 - V_b)$$
 (Eq 4)

$$M_{\rm S2} = M_{\rm S} - 564(x_Y - \bar{x}) \tag{Eq 5}$$

where  $x_b$  is the amount of the carbon trapped in the bainitic ferrites, assumed to be 0.03 wt.% (Ref 29),  $x_Y$  is the carbon concentration of the residual austenites,  $\bar{x}$  is the average carbon concentration of the alloy (for this steel is 0.4 wt.%),  $V_b$  is the volume fraction of bainitic ferrites,  $V_b$  is measured by the



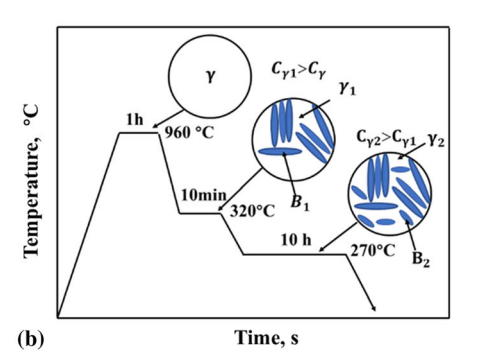


Fig. 1 The heat treatment procedure: (a) CIT, and (b) TIT ( $\gamma$ ,  $\gamma_1$ , and  $\gamma_2$  are the illustrating austenite microstructures in the austenitizing process, conventional isothermal bainitic transformation process, and two-step isothermal bainitic transformation process, respectively.  $C_{\gamma}$ ,  $C_{\gamma 1}$ , and  $C_{\gamma 2}$  are the carbon content corresponding to  $\gamma$ ,  $\gamma_1$ , and  $\gamma_2$ , respectively.  $B_1$  and  $B_2$  are the bainite microstructures in the conventional isothermal bainitic transformation process and two-step isothermal bainitic transformation process, respectively

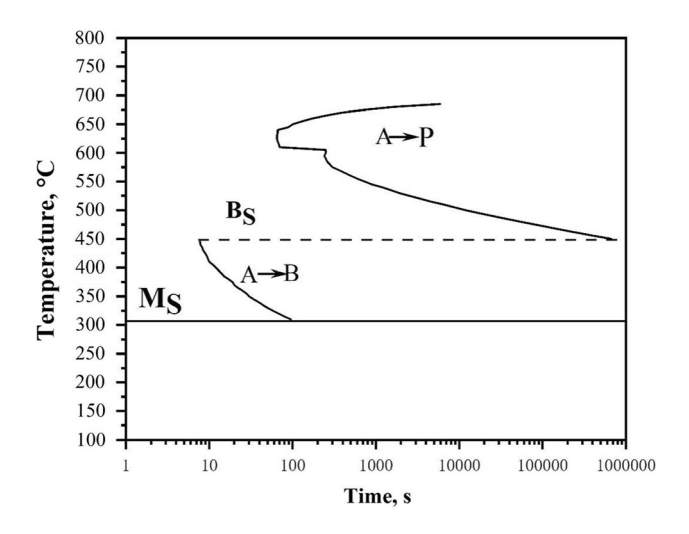


Fig. 2 Calculated TTT curves of the tested steel

Image Pro plus 6.0 (Ref 28) based on the difference between the martensites and the lower bainites in the OM images, and the volume percent of the bainites is about 60% when the test steel was isothermally transformed at 320 °C for 10 min. which is consistent with previous studies (Ref 30). There is a wellknown phenomenon that the martensitic transformation point has an important relationship with the carbon content in austenites. It is necessary to clarify the change of the carbon content in retained austenites during bainite transformation. When bainite transformation occurs, the carbon is distributed from bainites to RAs or precipitated as carbides, while other alloying elements are not (Ref 31). In order to reduce the competitive reaction of carbides, the previous studies (Ref 22-25) added a sufficient amount of silicon to the steels to suppress the precipitation of carbides, resulting in more carbon in the retained austenites. The carbon content in RAs can be calculated easily and accurately according to the law of mass conservation. But for the tested steels, there is not enough silicon to inhibit carbide precipitation. Therefore, it is unreasonable to calculate the carbon content in RAs by Eq 2. When considering the presence of carbides, the carbon partition follows the modified formula:

$$X_{\gamma} = (\overline{x} - V_{b}x_{b} - V_{\theta}x_{\theta})/(1 - V_{b}) \tag{Eq 6}$$

where  $V_{\theta}$  is the volume fraction of carbides, and by the measurement of  $V_{\theta}$  in scanning electron microscopy through the Image Pro plus 6.0 (Ref 28), the volume percent of the carbides is about 30%, when the test steel was isothermally transformed at 320 °C for 10 min.  $x_{\theta}$  is the carbon concentrations of the carbides, assumed to be 0.27 wt.% (Ref 12, 13). The calculated  $M_{\rm S2}$  temperature is 111.19 °C. Due to that some carbon allocated to defects is not easy to be detected (i.e., vacancies, dislocations, and interfaces) (Ref 32), the carbon in the untransformed austenites is less than the calculated value, causing the computing martensitic transformation point to be slightly lower than the actual martensitic transformation point.

## 3.2 Microstructures

Figure 3 reveals the microstructure differences subjected to two different heat treatment processes. The OM microstructures

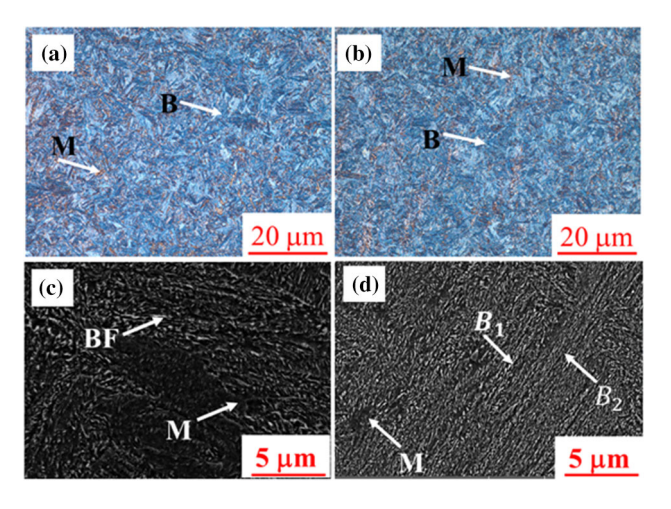


Fig. 3 The typical OM and SEM microstructures of: (a) and (c) CIT sample and (b) and, (d) TIT sample

obtained by the conventional isothermal bainitic transformation (CIT) and the two-step isothermal bainitic transformation (TIT) are presented in Fig. 3(a) and (b), respectively. As can been found, the obtained microstructure is differentiated into two distinct features of martensites (brown color) and lower bainites (blue color) (Ref 33). However, the carbides are too small to be detected by the OM observation and will be explored in TEM and SEM micrographs (Ref 30). The volume percent of bainites for CIT is 88%. In contrast, the volume percent of bainites for TIT is 92%. It is due to that the higher volume fractions of bainite sheaves can be obtained at lower transformation temperatures, which consume more primary austenites and decrease its average diameter. It is noted that the amount of the bainite transformation is higher than that of medium-carbon high-silicon steels (Ref 23) whether for CIT or TIT. This is because the tested steels do not have enough silicon contents to suppress carbide precipitation. Therefore, the carbon enrichment in RAs is not obvious, and hence, austenites are easier to transform into bainites than to stabilize at room temperature.

In order to better distinguish the microstructures of both processed samples, high-magnification SEM microstructures for both specimens, which are made and examined in the present work are exhibited in Fig. 3(c) and (d), respectively. The lower bainites and martensites are found in these microstructures together with carbides (Ref 30). It can be seen in this figure that different heat treatments produce bainitic ferrites with different thicknesses. Figure 3(c) displays the matrix of the sample conventionally austempered at 320 °C consisting of martensites and bainites, whereas the two-step austempering process has led to the formation of finer bainitic plates in the second stage  $(B_2)$ , as indicated with arrows in Fig. 3(d). The average plate size is less than that of the first stage  $(B_1)$  plates (Ref 22). The finer bainite  $(B_2)$  obtained can be primarily due to the lower transition temperature (a larger driving force at lower temperatures increases the nucleation rate) and higher austenite carbon contents (Ref 17). Unlike the previous study (Ref 23, 24, 27) on high-silicon steels, it is hard to find a great number of RAs. Due to the low Si content permitting the completion of the bainitic transformation, there is the precipitation of cementites and no RAs (Ref 34).

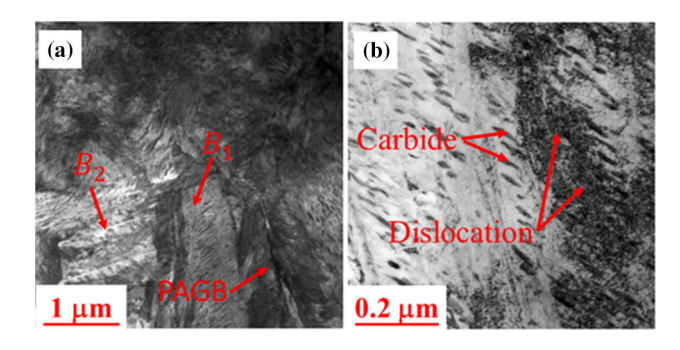


Fig. 4 The TEM microstructures of the TIT sample

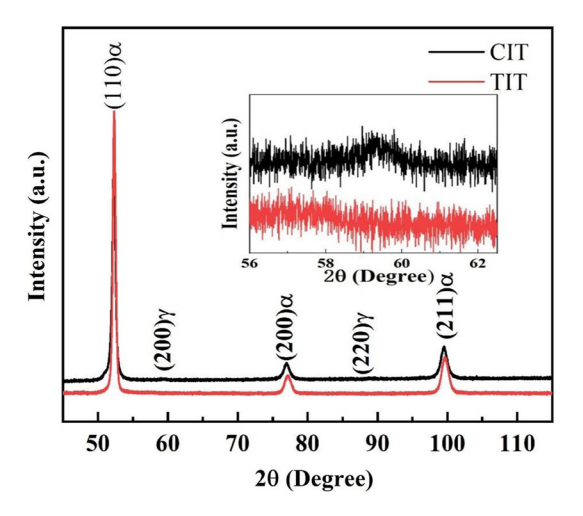


Fig. 5 XRD patterns for CIT and TIT samples

The TEM images of the TIT sample are displayed in Fig. 4. Figure 4(a) shows the lower bainite laths, which nucleate on the prior austenite grain boundaries (PAGBs), grow needle-shaped inside the grains and along the grain boundaries (Ref 30). Obviously, there are two different sizes of bainites produced by the TIT, which bear the same result, as observed by SEM. The  $B_1$  bainitic ferrite size is larger, compared to the  $B_2$  bainitic ferrite size. In addition, the carbide size in  $B_1$  is also larger than that in the  $B_2$ , which is due to finer bainitic ferrite plates, while the carbide-bearing bainites contain finer carbides (Ref 35). Figure 4(b) reveals that the fine carbides are mostly situated in the  $55^{\circ}$  direction with the longitudinal axes, which is a typical characteristic of the lower bainite microstructure (Ref 36).

Figure 5 illustrates the different diffraction peaks of CIT and TIT samples by XRD tests. The angles and the integrated intensities of different diffraction peaks are measured by the software of High-Score Plus (Ref 37). According to the results in Fig. 5, the amount of *RA*s is counted, based on Eq 7

$$V_i = 1/[1 + (G * I_\alpha)/I_\gamma]$$
 (Eq 7)

where the  $V_i$  in Eq 7 represents the amount of RAs for each diffraction peak and the value of G is selected according to the study by Wang et al. (Ref 38). 2.5 is for  $I_{\alpha}(200)/I_{\gamma}(200)$  and 1.2 for  $I_{\alpha}(211)/I_{\gamma}(200)$ . Here  $I_{\alpha}$  and  $I_{\gamma}$  represent the corresponding integrated intensities of ferrites and austenites, respectively. The  $V_{\gamma}$  of CIT is 3.1%. However, the  $V_{\gamma}$  of TIT is too low to be detected due to that RAs transform into much finer bainites at lower isothermal temperatures (Ref 22). The results of volume

Table 1 Mechanical properties of the studied steels

Sample	UTS, MPa	TEL, %	$A_{Kv}$ , J	$V_{\gamma}$
Conventional isothermal	1400	8.2	40	3.1
Two-step isothermal	1500	8.6	42	

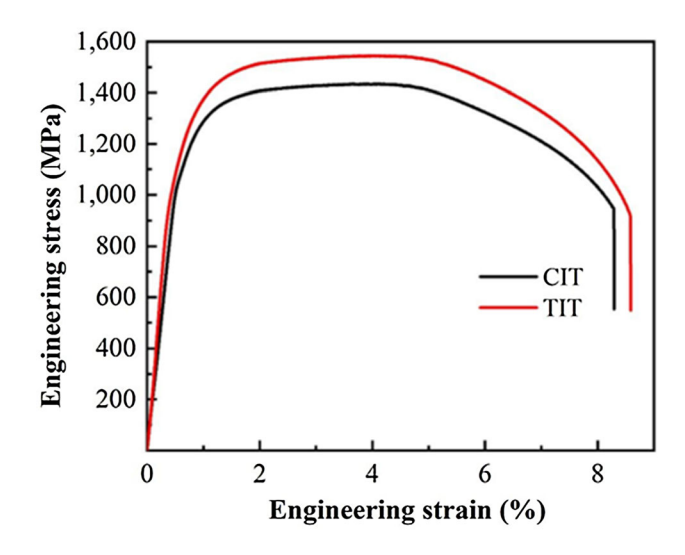


Fig. 6 The engineering stress-strain curves

fractions of retained austenites in TIT and CIT samples are listed in Table 1.

# 3.3 Mechanical Properties at Room Temperature

Figure 6 exhibits the engineering stress–strain curves of TIT and CIT samples, and the mechanical properties extracted from those curves are summarized in Table 1. The tensile strength ( $\sigma_b$ , 1400 MPa), total elongation (TEL, 8.2%), and impact toughness ( $A_{kv}$ , 40 J) are with the conventional bainites. From the view of Fig. 6, the product of strength and elongation of the two-step super-bainite is higher in comparison with the conventional bainites. Compared with the CIT sample, the tensile strength, elongation, and impact toughness in the TIT sample are increased by about 7.1, 4.9, and 5%, respectively.

#### 3.4 Wear Resistance

The calculation of the wear rate and the observation of the wear morphology are conducted for two different heat-treated samples in order to better compare their wear resistances. A smaller wear rate means a higher wear resistance, since it requires more energy to remove the same volume (Ref 39). The wear rate can be obtained by measuring the depth and width of the wear scars. Figure 7 compares the wear-scar profile diagrams of the TIT and CIT samples (a schematic diagram of the typical wear track profile is inserted in Fig. 7), and the results of the rolling-sliding specific wear rate for two samples are listed in Table 2. It deduced from Table 2 that the TIT sample has a lower wear rate than the CIT sample. The wear rates of the TIT and CIT samples in dry air are approximately  $0.36 \times 10^{-4}$  and  $1.46 \times 10^{-4}$  mm<sup>3</sup> N<sup>-1</sup> m<sup>-1</sup>, respectively. This trend indicates a fourfold difference in wear rates between

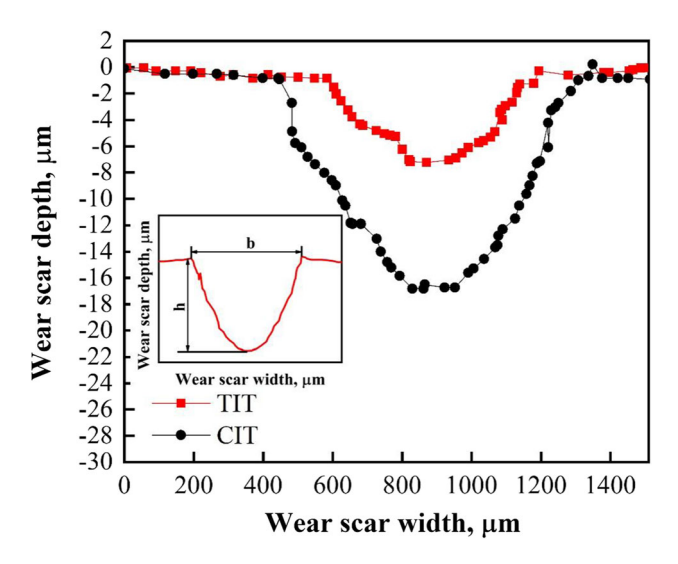


**Fig. 7** Line profiles of the wear scars of two different heat-treated samples. The inserted schematic diagram is the typical wear track profile, b and h represent the wear scar width and depth, respectively

Table 2 Hardness and wear rate of the tested steels

Sample	Hardness, HV	Specific wear rate, mm $^{-3}$ N $^{-1}$ m $^{-1}/10^{-4}$
Conventional isothermal	406.4	1.46
Two-step isother- mal	439.6	0.36

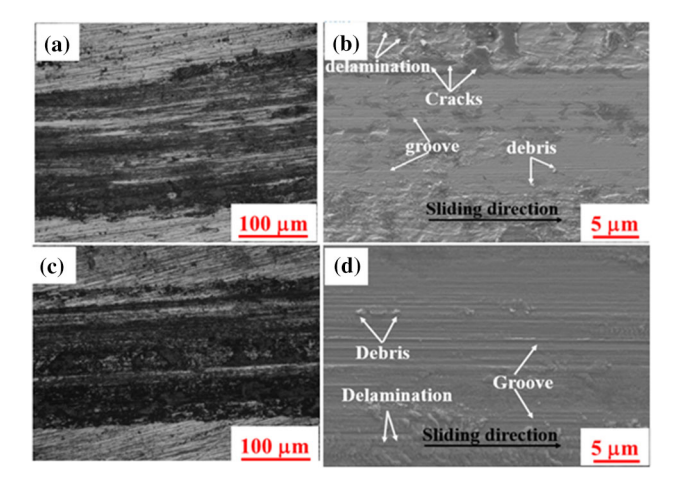


Fig. 8 The OM and SEM morphologies of wear surfaces: (a) and (b): CIT process, (c) and (d): TIT process

the two samples. And the hardness values of the TIT and CIT samples are 439.6 and 406.4 HV, respectively.

Figure 8 shows the SEM and OM images of the worn surface with different heat treatments under dry conditions. Distinct differences on wear-surface morphologies could be easily discerned with different heat treatments. Figure 8(a) and (b) corresponds to the OM and SEM images of the worn surface at CIT, respectively. As shown in Fig. 8(b), the plastic deformation along the groove, and the lamellar delamination

could be clearly found. Furthermore, dark areas are observed on the wear surface, indicating that the surface is subjected to the adhesive wear (Ref 40, 41). However, for the sample produced by TIT, as presented in Fig. 8(d), it can be demonstrated that there are many deep and wide plowing grooves parallel to the sliding direction, and the plastic deformation along the grooves happens. Moreover, it is also found to be a slight delamination, indicating that the wear mechanism of the TIT sample is the abrasive and delamination wears (Ref 42).

# 4. Discussion

#### 4.1 Improvement of Mechanical Properties by the TIT

As shown in Table 1, the TIT sample exhibits better mechanical properties of studied medium-carbon low-Si steels, compared with the CIT sample. The mechanical behavior of bainitic steels is mainly influenced by the volume fractions, morphologies, and distributions of bainites and RAs (Ref 43). According to the results of the OM, SEM, TEM, and XRD (Fig. 3, 4, and 5) analysis in the section, Sect. 3, the volume fractions of bainites and RAs have small difference between the TIT sand CIT samples. It seems unable to explain the enhancement of the mechanical behavior by the TIT. However, the SEM and TEM images manifest that the TIT sample produced the finer bainites  $(B_2)$  with the finer carbides. The  $B_1$ bainites size of the CIT sample is larger than the  $B_2$ , which only exists in the TIT sample. The strength of bainitic steels is mainly determined by several factors, such as the dislocation density in bainites, thickness of bainitic ferrites, distance between carbides, and alloying elements (Ref 29, 44). The bainite formation at low austempering temperatures results in higher dislocation densities and finer bainite laths (Ref 9). Therefore, the higher tensile strength (1500 MPa) of the TIT sample may stem from the finer microstructure and stronger  $B_2$ bainites, primarily. For the two-step isothermal sample, the elongation is slighly improved, compared with the conventional isothermal sample, which is attributed to the lack of the brittle martensite in the multi-step transformed samples (Ref 23). Blocky retained austenites (BRAs) were easily transformed to martensites, which have a deteriorating effect on plasticity. Unlike high-Si steels, not a few retained austenites are available in the tested steels. This is because the tested steels have carbide precipitates during the bainite transformation, which causes the untransformed austenite to partition enough carbon so that it is the martensite transformation point  $(M_S)$  that is above the room temperature and transforms into brittle martensite during subsequent cooling, In contrast, RAs in high-Si steels are more difficult to transform into brittle martensites at room temperature. This trend implies that the BRAs transformed into brittle martensites (due to that there are only a few RAs in the TIT and CIT samples) are not the main reason to account for the TIT sample having better elongation than the CIT sample. The reason for the toughness improvement may be related to the carbide size and the extent of the prior austenite grains refinement (Ref 45), and coarse bainites  $(B_1)$  with a coarser carbides size having a poor ductility in comparison with finer bainites  $(B_2)$  containing finer carbide sizes. Thus, the TIT sample, which has produced some finer bainites  $(B_2)$ , exhibits better toughness than the CIT sample.

# 4.2 Multiple Factors (Hardness, Toughness, Microstructures, and Carbides) Affecting the Wear Resistance

The TIT sample has better wear resistance by analyzing wear mechanisms and wear rates from Fig. 8 and Table 2. It is surprising that there is such a significant difference in the wear rates when the hardness values of the two samples are not much different. Thus, it is concluded that the wear rate can be closely related to other factors (Ref 46, 47), such as microstructures, work hardening, fracture, and fatigue properties. The microstructure is an important parameter affecting the abrasion behavior (Ref 48), and generally, the microstructures with a combination of hard and soft phases can impart plastic deformation, which is considered to be highly beneficial in abrasive applications (Ref 49, 50). The finer bainites  $(B_2)$ , which produce at a lower temperature (270 °C), compared to the coarser bainites  $(B_1)$ , are obtained at 320 °C. It mean that  $B_2$ has a higher dislocation density (Ref 29), and finer bainitic ferrite plates (Ref 23) [both are favorable for increasing yield strengths (Ref 35, 51)], are compared to  $B_1$ . Thus, the TIT sample consists of harder bainites  $(B_2)$  and softer bainites  $(B_1)$ , while the CIT sample has only the bainite austempering at 320 °C (the influence of martensites and retained austenites is ignored due to the very small volume fraction). The carbide size also strongly affects wear properties. The TEM results reveal that  $B_2$  bainites have finer carbides than  $B_1$  bainites, and the refinement of the carbides to improve the wear resistance is similarly observed in tempered martensites. According to Deng et al. (Ref 52), a large number of small-sized carbides provide the highest wear resistance, while when the number density of carbides is small or the size is larger, the steels exhibit relatively lower wear resistance. Moreover, the TIT sample has a higher toughness, which can limit cracks formation (Ref 53) and contribute to increasing wear properties (Ref 54).

# 5. Conclusions

In the present work, CIT and TIT have been conducted on a medium-carbon low-Si steel. The influences of this process on mechanical and wear properties are investigated. The following findings could be obtained from the present work:

- Two different generations of bainites (B<sub>1</sub> and B<sub>2</sub>) are present in the TIT sample, whereas only B<sub>1</sub> bainites are presented in the CIT sample. Unlike the high-Si steels, the tested steels have a very low retained austenite content through either TIT or CIT.
- 2. Compared with CIT, the TIT sample has better mechanical properties, including the higher tensile strength, hardness, elongation, and impact toughness. The formation of finer bainites (*B*<sub>2</sub>) is the dominant factor in increasing the tensile strength. Unlike high-Si steels, finer carbides are the main reasons in increasing the elongation rather than the significant decrease in the volume fraction of *BRAs*, due to that there are a few *RAs* in TIT and CIT samples.
- 3. The two-step isothermal sample has a lower wear rate than the conventional isothermal sample. The TIT sample is of the abrasive and delamination wears, while the CIT sample is of the adhesive wear. It indicates that the twostep isothermal sample has better wear resistance, com-

pared with the conventional isothermal sample. Higher hardness is not the only factor for the difference in the wear resistance between two heat-treated samples. The toughness, microstructures with a combination of hard and soft phases, and finer carbides in  $B_2$  bainites of the TIT sample are responsible for the better wear resistance.

#### Acknowledgments

The authors would like to acknowledge the financial support of the National Natural Science Foundation of China (No. 52271110). P.K.L very much appreciates the supports from the National Science Foundation (DMR- 1611180 and 1809640).

#### References

- C. Garcia-Mateo, F.G. Caballero, and H.K.D.H. Bhadeshia, Development of Hard Bainite, ISIJ Int., 2003, 43, p 1238–1243.
- F.G. Caballero, H.K.D.H. Bhadeshia, K.J.A. Mawella, D.G. Jones, and P. Brown, Very Strong Low Temperature Bainite, *Mater. Sci. Technol.*, 2002, 18, p 279–284.
- C. Garcia-Mateo, F. Caballero, and H. Bhadeshia, Low Temperature Bainite, J. Phys. IV Frnace, 2003, 112, p 285–288. https://doi.org/10. 1051/jp4:2003884
- C. Garcia-Mateo, F.G. Caballero, and H.K.D.H. Bhadeshia, Acceleration of Low-Temperature Bainite, ISIJ Int., 2003, 43, p 1821–1825.
- S. Das Bakshi, P.H. Shipway, and H.K.D.H. Bhadeshia, Three-Body Abrasive Wear of Fine Pearlite, Nanostructured Bainite and Martensite, Wear, 2013, 308, p 46–53.
- S.M. Hasan, D. Chakrabarti, and S.B. Singh, Dry Rolling/Sliding Wear Behaviour of Pearlitic Rail and Newly Developed Carbide-Free Bainitic Rail Steels, Wear, 2018, 408–409, p 151–159.
- W. Liu, Y.H. Jiang, H. Guo, Y. Zhang, A.M. Zhao, and Y. Huang, Metallurgy, Materials: Mechanical Properties and Wear Resistance of Ultrafine Bainitic Steel under Low Austempering Temperature, Int. J. Miner. Metall. Mater., 2020, 27, p 483

  –493.
- Q. Luo, J. Li, Q. Yan, W. Li, and Y. Ding, Sliding Wear of Medium-Carbon Bainitic/Martensitic/Austenitic Steel Treated by Short-Term Low-Temperature Austempering, Wear, 2021, 476, p 203732.
- H. Bhadeshia and J.W. Christian, Bainite in Steels, Metall. Trans. A, 1990, 21, p 767–797.
- I.B. Timokhina, P.D. Hodgson, and E.V. Pereloma, Effect of Microstructure on the Stability of Retained Austenite in Transformation-Induced-Plasticity Steels, *Metall. Mater. Trans. A*, 2004, 35, p 2331–2341
- E.V. Pereloma, I.B. Timokhina, M.K. Miller, and P.D. Hodgson, Three-Dimensional Atom Probe Analysis of Solute Distribution in Thermomechanically Processed TRIP Steels, *Acta Mater.*, 2007, 55, p 2587– 2598.
- H.K.D.H. Bhadeshia and D.V. Edmonds, Bainite in Silicon Steels: New Composition-Property Approach Part 1, *Met. Sci.*, 1983, 17, p 411– 419.
- H.K.D.H. Bhadeshia and D.V. Edmonds, Bainite in Silicon Steels: New Composition-Property Approach Part 2, Met. Sci., 1983, 17, p 420– 425.
- S.A. Podder, I. Lonardelli, A. Molinari, and K.H.D.H. Bhadeshia, Thermal Stability of Retained Austenite in Bainitic Steel: An In Situ Study, Proc. R. Soc. A Math. Phys. Eng. Sci., 2011, 467, p 3141–3156.
- E. Bonnevie, G. Ferrière, A. Ikhlef, D. Kaplan, and J.M. Orain, Morphological Aspects of Martensite–Austenite Constituents in Intercritical and Coarse Grain Heat Affected Zones of Structural Steels, *Mater. Sci. Eng. A*, 2004, 385, p 352–358.
- F. Caballero, M. Santofimia, C. Capdevila, C. Garcia-Mateo, and C. García de Andrés, Design of Advanced Bainitic Steels by Optimisation of TTT Diagrams and T0 Curves, ISIJ Int., 2006, 46, p 1479–1488.
- S.B. Singh and H.K.D.H. Bhadeshia, Estimation of Bainite Plate-Thickness in Low-Alloy Steels, *Mater. Sci. Eng. A*, 1998, 245, p 72–79.

- G. Fourlaris and G. Papadimitriou, TEM Microscopical Examination of the Stepped Bainite Reaction in Silicon Steels, *Microsc. Microanal.*, 1997, 3, p 689–690.
- K. Zhu, O. Bouaziz, C. Oberbillig, and M. Huang, An Approach to Define the Effective Lath Size Controlling Yield Strength of Bainite, *Mater. Sci. Eng. A*, 2010, 527, p 6614–6619.
- K. Singh and A. Singh, Tribological Response and Microstructural Evolution of Nanostructured Bainitic Steel under Repeated Frictional Sliding, Wear, 2018, 410–411, p 63–71.
- H. Guo, A. Zhao, C. Zhi, R. Ding, and J. Wang, Two-Body Abrasion Wear Mechanism of Super Bainitic Steel, *Mater. Sci. Technol.*, 2017, 33, p 893–898.
- K. Hase, C. Garcia-Mateo, and H.K.D.H. Bhadeshia, Bimodal Size-Distribution of Bainite Plates, *Mater. Sci. Eng. A*, 2006, 438–440, p 145–148
- X.L. Wang, K.M. Wu, F. Hu, L. Yu, and X.L. Wan, Multi-step Isothermal Bainitic Transformation in Medium-Carbon Steel, Scr. Mater., 2014, 74, p 56–59.
- K.-W. Kim, K. Il Kim, C.-H. Lee, J.-Y. Kang, T.-H. Lee, K.-M. Cho, and K.H. Oh, Control of Retained Austenite Morphology through Double Bainitic Transformation, *Mater. Sci. Eng. A*, 2016, 673, p 557– 561
- J. Tian, G. Xu, Z. Jiang, M. Zhou, H. Hu, and Q. Yuan, Transformation Behavior of Bainite during Two-Step Isothermal Process in an Ultrafine Bainite Steel, *ISIJ Int.*, 2018, 58, p 1875–1882.
- M. Franceschi, A. Miotti Bettanini, L. Pezzato, M. Dabalà, and P.J. Jacques, Effect of Multi-step Austempering Treatment on the Microstructure and Mechanical Properties of a High Silicon Carbide-Free Bainitic Steel with Bimodal Bainite Distribution, *Metals*, 2021, 11, p 2055.
- H. Mousalou, S. Yazdani, B. Avishan, N.P. Ahmadi, A. Chabok, and Y. Pei, Microstructural and Mechanical Properties of Low-Carbon Ultrafine Bainitic Steel Produced by Multi-step Austempering Process, *Mater. Sci. Eng. A*, 2018, 734, p 329–337.
- M. Liu, G. Xu, J. Tian, Q. Yuan, and X. Chen, Effect of Austempering Time on Microstructure and Properties of a Low-Carbon Bainite Steel, *Int. J. Miner. Metall. Mater.*, 2020, 27, p 340–346.
- C.H. Young and H.K.D.H. Bhadeshia, Strength of Mixtures of Bainite and Martensite, *Mater. Sci. Technol.*, 1994, 10, p 209–214.
- S. Bakhshi and A. Mirak, The Effect of Low Temperature Transformation Time on Microstructural and Textural Evolution, Mechanical Properties and Fracture Behavior of a Low Alloy, Medium Carbon, Super Strength AISI 4340 Steel, Mater. Sci. Eng. A, 2022, 831, p 142247.
- F.G. Caballero, M.K. Miller, C. Garcia-Mateo, C. Capdevila, and S.S. Babu, Redistribution of Alloying Elements during Tempering of a Nanocrystalline Steel, *Acta Mater.*, 2008, 56, p 188–199.
- R. Rementeria, J.A. Jimenez, S.Y.P. Allain, G. Geandier, J.D. Poplawsky, W. Guo, E. Urones-Garrote, C. Garcia-Mateo, and F.G. Caballero, Quantitative Assessment of Carbon Allocation Anomalies in Low Temperature Bainite, *Acta Mater.*, 2017, 133, p 333–345.
- E. Girault, P. Jacques, P. Harlet, K. Mols, J. Van Humbeeck, E. Aernoudt, and F. Delannay, Metallographic Methods for Revealing the Multiphase Microstructure of TRIP-Assisted Steels, *Mater. Charact.*, 1998, 40, p 111–118.
- M. Masoumi, G. Tressia, D.M.A. Centeno, and H. Goldenstein, Improving the Mechanical Properties and Wear Resistance of a Commercial Pearlitic Rail Steel Using a Two-Step Heat Treatment, Metall. Mater. Trans. A, 2021, 52, p 4888–4906.
- X.Y. Long, F.C. Zhang, J. Kang, Z.N. Yang, D.D. Wu, K.M. Wu, and G.H. Zhang, Study on Carbide-Bearing and Carbide-Free Bainitic Steels and Their Wear Resistance, *Mater. Sci. Technol.*, 2016, 33, p 615–622.
- C. Gupta, G.K. Dey, J.K. Chakravartty, D. Srivastav, and S. Banerjee, A Study of Bainite Transformation in a New CrMoV Steel under Continuous Cooling Conditions, Scr. Mater., 2005, 53, p 559–564.
- Z. Yao, M. Liu, H. Hu, J. Tian, and G. Xu, Microstructure and Wear Properties of a Bainite/Martensite Multi-phase Wear Resistant Steel, ISLJ Int., 2021, 61, p 434–441.

- C.Y. Wang, J. Shi, W.Q. Cao, and H. Dong, Characterization of Microstructure Obtained by Quenching and Partitioning Process in Low Alloy Martensitic Steel, *Mater. Sci. Eng. A*, 2010, 527, p 3442– 3449
- J.-M. Wu, S.-J. Lin, J.-W. Yeh, S.-K. Chen, Y.-S. Huang, and H.-C. Chen, Adhesive Wear Behavior of AlxCoCrCuFeNi High-Entropy Alloys as a Function of Aluminum Content, Wear, 2006, 261, p 513– 519
- W. Qin, J. Li, Q. Mao, Y. Liu, Y. Liu, W. Jiang, and J. Kang, Evolution of Tribological Mechanisms of Nano-grained 304L Stainless Steel under Dry and Polyalphaolefin Lubrication Conditions, *Mater. Lett.*, 2019, 242, p 147–151.
- M.T. Umemura, L.B. Varela, C.E. Pinedo, R.C. Cozza, and A.P. Tschiptschin, Assessment of Tribological Properties of Plasma Nitrided 410S Ferritic-Martensitic Stainless Steels, Wear, 2019, 426–427, p 49–58.
- L.W. Lan, X.J. Wang, R.P. Guo, H.J. Yang, and J.W. Qiao, Effect of Environments and Normal Loads on Tribological Properties of Nitrided Ni<sub>45</sub>(FeCoCr)<sub>40</sub>(AlTi)<sub>15</sub> High-Entropy Alloys, *J. Mater. Sci. Technol.*, 2020, 42, p 85–96.
- M.N. Yoozbashi, S. Yazdani, and T.S. Wang, Design of a New Nanostructured, High-Si Bainitic Steel with Lower Cost Production, *Mater. Des.*, 2011, 32, p 3248–3253.
- A. Kumar and A. Singh, Mechanical Properties of Nanostructured Bainitic Steels, *Materialia*, 2021, 15, p 101034.
- R. Kannan, Y. Wang, M. Nouri, D. Li, and L. Li, Instrumented Indentation Study of Bainite/Martensite Duplex Microstructure, *Mater. Sci. Eng. A*, 2018, 713, p 1–6.
- P. Zhang, F.C. Zhang, Z.G. Yan, T.S. Wang, and L.H. Qian, Wear Property of Low-Temperature Bainite in the Surface Layer of a Carburized Low Carbon Steel, Wear, 2011, 271, p 697–704.
- 47. T.T. Matsuo, C.S. Kiminami, W.J.B. Fo, and C. Bolfarini, Sliding Wear of Spray-Formed High-Chromium White Cast Iron Alloys, *Wear*, 2005, **259**, p 445–452.
- D.A. Rigney, L.H. Chen, M.G.S. Naylor, and A.R. Rosenfield, Wear Processes in Sliding Systems, Wear, 1984, 100, p 195–219.
- V.G. Efremenko, K. Shimizu, T. Noguchi, A.V. Efremenko, and Y.G. Chabak, Impact–Abrasive–Corrosion Wear of Fe-Based Alloys: Influence of Microstructure and Chemical Composition Upon Wear Resistance, *Wear*, 2013, 305, p 155–165.
- B. Narayanaswamy, P. Hodgson, and H. Beladi, Comparisons of the Two-Body Abrasive Wear Behaviour of Four Different Ferrous Microstructures with Similar Hardness Levels, *Wear*, 2016, 350–351, p 155–165.
- Q. Zhou, L. Qian, J. Meng, L. Zhao, and F. Zhang, Low-Cycle Fatigue Behavior and Microstructural Evolution in a Low-Carbon Carbide-Free Bainitic Steel, *Mater. Des.*, 2015, 85, p 487–496.
- X.T. Deng, T.L. Fu, Z.D. Wang, R.D.K. Misra, and G.D. Wang, Epsilon Carbide Precipitation and Wear Behaviour of Low Alloy Wear Resistant Steels, *Mater. Sci. Technol.*, 2016, 32, p 320–327.
- S.D. Bakshi, Wear of Fine Pearlite, Nanostructured Bainite and Martensite, Wear, 2013, 308, p 46–53.
- A. Leiro, E. Vuorinen, K.G. Sundin, B. Prakash, T. Sourmail, V. Smanio, F.G. Caballero, C. Garcia-Mateo and R. Elvira, Wear of Nanostructured Carbide-Free Bainitic Steels under Dry Rolling-Sliding Conditions, *Wear*, 2013, 298–299, p 42–47.

**Publisher's Note** Springer Nature remains neutral with regard to jurisdictional claims in published maps and institutional affiliations.

Springer Nature or its licensor (e.g. a society or other partner) holds exclusive rights to this article under a publishing agreement with the author(s) or other rightsholder(s); author self-archiving of the accepted manuscript version of this article is solely governed by the terms of such publishing agreement and applicable law.